

# Evaluation of a T-wall Section in New Orleans Considering 3D Soil-Structure Interaction

Jinoh Won<sup>1</sup>, Sudarshan Adhikari<sup>2</sup>, Chung R. Song<sup>3</sup>, Alex H.-D. Cheng<sup>4</sup> and Ahmed Al-Ostaz<sup>5</sup>

1. Post Doctoral Research Associate, Civil Engineering, University of Mississippi, University, MS 38677, E-mail: [jwon@olemiss.edu](mailto:jwon@olemiss.edu)
2. Ph. D. Student, Civil Engineering, University of Mississippi, University, MS 38677, E-mail: [sadhikar@olemiss.edu](mailto:sadhikar@olemiss.edu)
3. Associate Professor, Civil Engineering, University of Mississippi, University, MS 38677, E-mail: [csong@olemiss.edu](mailto:csong@olemiss.edu)
4. Dean, School of Engineering, University of Mississippi, University, MS 38677, E-mail: [acheng@olemiss.edu](mailto:acheng@olemiss.edu)
5. Associate Professor, Civil Engineering, University of Mississippi, University, MS 38677, E-mail: [alostaz@olemiss.edu](mailto:alostaz@olemiss.edu)

## Abstract

T-walls in New Orleans appeared to survive hurricane Katrina while I-walls failed in several sections. However, it is still unclear whether these T-walls truly survived the hurricane with fair amount of safety margins or barely survived it with hidden damages.

The initial design of T-walls is based on rather oversimplified loading conditions with limited consideration of soil structure interaction. In this study, rigorous 3D numerical analyses are conducted incorporating realistic loading conditions and rigorous soil-structure interactions but with time saving techniques to evaluate the detailed behavior of T-walls.

This paper addressed the procedure of innovative 3D numerical analyses and important findings using special structural elements in FLAC<sup>3D</sup>. From this study, T-walls are found to have adequate stress levels in H-piles and concrete walls. However, it showed that the major factor that may cause the instability of the T-wall is the slope instability type rotational force that could not be considered in the initial design. This unexpected rotational force, however, was counteracted by the batter piles so that the overall integrity of the T-wall system is maintained.

## **Introduction**

Flood protection system in New Orleans is composed of earthen levees, I-walls, T-walls and pump stations. Earthen levees are deployed in areas where enough open land is available so that full size levees can be built. I-walls are deployed in areas where enough land is not available for full size earthen levees; concrete I-type floodwalls are built on the top of existing earthen levees so that additional water can be retained. Pile founded T-walls are deployed in areas such as pump stations and gates where more reliable and stronger walls than I-walls are required.

T-walls in New Orleans are supported by two to four rows batter piles to resist the water pressure (USCOE 2008), and they appeared to survive hurricane Katrina while I-walls failed in several places. However, it is not clear whether these T-walls truly survived the hurricane with appropriate safety margins or barely survived it with hidden damages because the design of existing T-walls (USCOE, 1967) was based on rather oversimplified design concepts assuming the water pressure was the only lateral force acting on the wall and disregarding the potential lateral force caused by the slope instability. The design also adopted Hrennikoff (1949) and Vetter's (1939) methods where piles were represented as normal, transverse and rotational springs immediately below the base of T-walls, in which pile and soil interaction at deeper grounds was disregarded. Reevaluation of T-walls including additional lateral force from the slope instability and group pile analysis (CPGA software) was conducted by USCOE (2008). The additional lateral force was computed from limit equilibrium condition, but the deformation due to the lateral force and associated soil-pile reaction was not fully incorporated. By default, the theory considered the lateral movement only above the anticipated failure line; it implicitly assumed zero lateral movement below the anticipated failure line. Therefore, the additional

lateral force from the limit equilibrium theory was assumed to distribute uniformly on the pile only above the anticipated failure line, which may be different from actual field conditions. Furthermore, CPGA computes the group effects by using predetermined reduction factors, not by recognizing and incorporating the pile and soil interaction (ref. ).

Therefore, a detailed evaluation of the performance of T-walls with detailed loading condition and full three dimensional soil-structure interactions and must be conducted to understand the realistic behavior of T-walls. But, the detailed evaluation of T-wall sections is extremely difficult due to the complicated loading conditions and associated 3D soil-pile-concrete wall interaction.

In this study, the behavior of T-walls is rigorously investigated using a 3D numerical technique based on FLAC<sup>3D</sup> (Itasca, 2006), which addresses the performance of T-walls in terms of the stresses of piles, lateral deformation of piles, stress of concrete walls and 'flow through' which is a phenomenon caused by weak soils passing through piles.

### **T-wall and soil profile in IHNC, New Orleans**

Fig. 1 shows the cross section of a T-wall, levee and soil stratigraphy. The T-wall system studied in this paper is not a specific T-wall section in a specific location, but it is a representative one constructed in IHNC (Inner Harbor Navigation Canal) area in New Orleans (USCOE 2008). This T-wall is supported by three rows batter H-piles (HP 14×73: Width 0.37 m, Depth 0.35 m). Piles in the first row are inclined leftward with 3:1 (V:H) inclination whereas piles in the second and third rows are inclined rightward with the same inclination. The pile tips rest on the medium-dense sand (SP) layer at EL. -27.7 m. The pile spacing along the out-of-plane

direction is 1.5 m which corresponds to  $4.1B$  ( $B$  = flange width of the H-pile). Sheet piles (PZ 22) are installed to reduce the water seepage across the levee. Shear strength parameters of each layer in Fig. 1 are obtained from USCOE (2008) and IPET (2007) and shown in Table 1. First layer (GL. to EL. -4.3 m) is a highly compressible clay (CH) layer with the undrained shear strength  $5.7 \text{ kN/m}^2$ . Geomatrix (2007) describes it as a peat layer. Second layer (EL. -4.3 m to EL. -26.2 m) is generally classified as CH, but it includes a thin silty clay (ML) layer from EL. -7.0 ~ EL. -7.9 m. The average undrained shear strength of the second clay layer ranges 9.6 to  $37.8 \text{ kN/m}^2$  with undrained shear strength to depth ratio  $1.3 \text{ kN/m}^2/\text{m}$ . Sand layer (SP) follows the clay layer with the internal friction angle  $30^\circ$ . The levee materials sit on the peat layer with the undrained shear strength  $23.9 \text{ kN/m}^2$ .

Soil moduli are obtained using correlations between the undrained shear strength and undrained moduli. In this study,  $G/s_u$  ratios 100 to 160 are used referring to Geomatrix (2007), HPO-Hurricane Protection Office (2008) and Adhikari et al. (2009). Shear modulus of the sand layer is taken from Geomatrix (2007). Bulk moduli ( $K$ ) are estimated from shear modulus ( $G$ ) and the Poisson's ratio. Poisson's ratio 0.48 is used for clay layers by assuming that the soil is mostly saturated. Poisson's ratio 0.3 is used for the sand layer.

The initial vertical soil stress is computed from the unit weight and depth. However, the horizontal soil stress is computed with careful engineering evaluation as follows. The total initial horizontal stress is computed from the summation of the effective horizontal stress based on the at-rest earth pressure coefficient and water pressure. However, the total stress analysis does not distinguish the effective stress and water pressure, and therefore, the initial total horizontal stress cannot be computed accurately using the total stress analysis. To overcome this technical issue,

this study computed the equivalent at-rest earth pressure coefficient by taking the weighted average of effective lateral pressure and water pressure as follow;

$$K_o' = \frac{\sum K_o \gamma' h_i + \gamma_w \sum h_i}{\sum \gamma_{sat} h_i} \quad (1)$$

where,  $K_o$  is the at-rest earth pressure coefficient of soils,  $\gamma'$  and  $\gamma_{sat}$  is the effective unit weight and saturated unit weight,  $\gamma_w$  is the unit weight of water, and  $h_i$  is the height of each soil layer. Most soil layers in New Orleans are in normally consolidated or lightly overconsolidated (IPET, 2007) condition, so that  $K_o$  value may be estimated using Jaky's (1944) equation ( $K_o = 1 - \sin\phi$ ). The computed  $K_o'$  for soils in Fig. 1 and Table 1 turned out to be 0.83. Therefore,  $K_o' = 0.83$  is used in this study for the initial stress computation.

### **Evaluation of soil-structure interaction spring constants**

To reduce the computation time in modeling the piles, 'pile elements' are used in this study as shown in Fig. 2. They are line elements with coupling springs representing the interaction between piles and soils. Line elements are free from nodal connectivity of surrounding solid elements, and the batter piles can be easily modeled compared to three dimensional solid elements.

FLAC recognizes the coupling springs as elastic-perfectly plastic models as shown in Fig. 3. Therefore, the initial slope and the yield point should be defined. This study used the following relations for assessing shear spring constants,

$$\frac{F_s^{\max}}{L} = (c_s + K_o \sigma'_v \cdot \tan \delta) \cdot P_e \quad (2-1)$$

$$= c_s \cdot P_e = (\alpha \cdot s_u) \cdot P_e \quad \text{for clay} \quad (2-2)$$

$$= (K_o \sigma'_v \cdot \tan \delta) \cdot P_e \quad \text{for sand} \quad (2-3)$$

where,  $F_s^{\max}$  is the maximum shear force,  $L$  is the length of a pile element for a selected soil layer,  $c_s$  is the cohesion,  $K_o$  is the lateral earth pressure coefficient,  $\sigma'_v$  is the effective overburden pressure,  $p_e$  is the perimeter,  $\alpha$  is the adhesion constant and it is assumed 1 as recommended by USCOE (1991),  $s_u$  is the undrained shear strength, and  $\delta$  is the angle of friction between soil and pile and it is assumed  $0.75\phi$  as recommended by USCOE (1991). The shear spring is determined from the initial slope of  $F_s/L$  vs. displacement relationship (Fig. 3) where the asymptotic point is obtained when the displacement is  $0.01B$  ( $B =$  pile diameter) for clay (Reese and O'Neill, 1988) and  $0.03B$  for sandy soil (Coyle and Sulaiman, 1967).

For the evaluation of normal coupling spring constants, it is noted that the pile in a T-wall is a typical 'passive pile' (a pile subjected to lateral soil movement). Therefore, the maximum normal force per unit length ( $F_n^{\max}/L$ ) is obtained from the numerical analysis of a passive pile as shown in Fig. 4. The lateral force caused by soil movement acting on the pile is calculated as the soil moves laterally with applied constant velocity ( $1.5 \times 10^{-6}$  m/step). Using the computed force acting on the pile and the displacement,  $F_n^{\max}/L$  and a normal spring constant ( $k_n$ ) are computed from the slope in Fig. 3. Using  $F_n^{\max}/L$  at eight different depths,  $F_n^{\max}/L$  vs.  $\sigma'_m \cdot p_e$

relationships are plotted as shown in Fig. 5, and  $c_n$  and  $\phi_n$  are computed using the following relationship,

$$\frac{F_n^{\max}}{L} = c_n + \sigma'_m \cdot p_e \cdot \tan \phi_n \quad (3)$$

where,  $F_n^{\max}$  is the maximum normal force,  $L$  is the length of a pile element for a selected soil layer,  $c_n$  is the cohesion constant (not the cohesion itself),  $\sigma'_m$  is the mean principle stress,  $p_e$  is the perimeter, and  $\phi_n$  is the slope of a line in Fig. 5. Different abscissa and slopes were taken for different layers to reflect different soil conditions. The summary of shear and normal spring constants is shown in Table 2.

The computed  $F_n^{\max} / L$  is also compared with ultimate lateral resistance of soils (typically noted as  $P_u$ ) because  $F_n^{\max} / (L \cdot B_{pile})$  (where,  $B_{pile}$  is the diameter of a pile) is the same as  $P_u$ . This study showed  $P_u \approx 9 s_u$  for circular piles and  $P_u \approx 15 s_u$  for rectangular piles, which agreed well with published results (Chen 1994, Bransby and Spring 1999, Chen and Martin 2002, Pan et al. 2002, Broms 1964, Matlock 1970, and Randolph and Houslby 1984).

The sheet pile is modeled using 'embedded liner element' in FLAC<sup>3D</sup>, which is a modified shell element including the capability of incorporating sliding and gap development between the sheet pile and soil. In this case, strength properties are important, but elastic properties are not. Therefore, the lowest stiffness consistent with small interface deformation is desirable, and the maximum interface spring constants are defined as follows as recommended by ITASCA (2006);

$$k_s \approx k_n \approx 10 \cdot \left[ \frac{(K + 4/3G)}{\Delta z_{\min}} \right] \quad (4)$$

where,  $\Delta z_{\min}$  is the smallest width of an adjoining zone in the normal direction, and K and G are the bulk modulus and shear modulus of soil, respectively.

The concrete wall and base of the T-wall are modeled using solid elements. Reinforcement is considered by taking the weighted average of the steel and concrete. Around the concrete block, interface elements are used to simulate the interaction between the concrete and the soil, so that the gapping and slippage are considered at the interface. The same interface springs used for sheet piles are used.

End bearing spring constant is estimated ( $k=48.0$  MN/m) from the ultimate bearing capacity based on Meyerhof (1976) for  $\phi=30^\circ$  (Ultimate End Bearing= $535.0$  kN/m<sup>2</sup> for the sand layer in Table 1) and the critical deformation  $0.03B$  to  $0.08B$  ( $0.04 \sim 0.10$  inches) (because Reese and O'Neill (1989) reported no clearly defined critical deformation for sandy soils). The lateral normal spring constant and shear spring constant at the pile tip are estimated as the same manner as in the case of the pile shaft. The frictional resistance between the pile tip and supporting soils is disregarded. The computed spring constants did not show much variation for different critical deformation, therefore, the spring constants computed from  $0.03B$  deformation was used for further study.

The connection between the piles and pile cap is assumed a continuous reinforced concrete considering that the reinforced concreted pad was casted on the top of the piles. The summary of input parameters including the data for steels and concrete for FLAC simulation is shown Table 3.

## **Performance evaluation of the pile element**

The performance of pile elements with estimated spring constants is evaluated by comparing the results to a full 3D solid element analyses for a single pile. Fig. 6 shows two meshes used for the analyses and comparison of a single passive pile; one is a very fine mesh using 3D solid elements, and another one is a coarse mesh using pile elements.

To simulate the field loading condition,  $29.4 \text{ kN/m}^2$  hydraulic pressure that corresponds to 3 m water head is applied on the ground surface, left side of the pile. The pressure is applied incrementally starting from the water level of 0.6 m and to 1.2, 1.8, 2.4 and 3 m water level.

Fig. 7 shows that the displacements obtained from the pile elements and from the solid elements are essentially identical. The computation time for a mesh with pile elements is about one fifth that for a mesh with full 3D solid elements. Therefore, it shows that pile elements with proper spring constants can be used to simulate the 3D behavior of lateral piles with substantially reduced computation costs.

## **3D Numerical simulations of T-wall system and Results**

To obtain the realistic field condition, the construction sequence of the levee, sheet piles, and T-wall is followed. Elastic behavior of concrete and steel piles is assumed while Mohr-Coulomb yield criterion and undrained condition is applied for soils (admitting that the simulation should be conducted again with proper plasticity for concrete and steel member if these members exhibit the inelastic behavior, but it turned the all concrete and steel members

exhibited the elastic behavior). Then, the deformations are set to zero but the stresses are kept to establish the proper initial condition. The hydraulic pressure is applied not only on the ground surface of the flood side but also on the floodwall itself. The load is applied with 0.6 m water level increment from 0 m and to 3 m as mentioned previously to avoid numerical problems.

The details of a T-wall structure and its 3D mesh are shown in Fig. 8. Total three rows of H-piles are installed to support the T-wall. Pile element in FLAC<sup>3D</sup> is used for the batter H-piles with the estimated shear and normal coupling-spring constants addressed in previous sections. It is also assumed that the behavior of batter piles is similar to that of vertical pile.

### *Deformation and pile stress*

Fig. 9 shows the overall deformation shape and displacement contour for 3 m water level condition in IHNC. It shows that the water pressure on the river side caused the rotational motion of the whole levee structure, resulting in some heaving at the protected side of the levee and inward tilting of the flood wall. Particularly, the inward tilting of the flood wall indicates that the overall soil rotation underneath the T-wall is the governing factor of the critical instability, not the lateral deformation of the concrete wall due to the water pressure. This rotational motion conceptually agrees well with critical failure surface predicted by the limit equilibrium, but not with the conventional design concepts (USCOE, 1967) which did not consider the slope stability problems.

It is noted again that the numerical analysis was performed for undrained conditions; the increased water level is incorporated as hydrostatic pressure acting on the surface of the river bed and any dissipation of excess pore pressure during the water level increase is not considered. The

obtained result, therefore, should be interpreted as a worst case result. Considering that it took approximately 30 hours for the water level in the canal to reach up to EL. 3.0m level (IPET, 2007) and soils in the area are mostly clayey soils (CH), the undrained assumption is a reasonable one.

Fig. 10 shows the distribution of lateral soil stresses acting on all three pile shafts; these are additional to the in situ initial soil stress. The solid lines represent computed normal stresses in this study. The computed lateral stress shows peaks from EL. -3.0 to -6.0 m. These high stresses are believed to be caused mostly due to the high rotational motion observed in Fig. 9. The lateral stress acting on the sheet pile is essentially zero, and the numerical simulation without the sheet pile showed about the same results as Fig. 10.

The dotted lines represent the anticipated normal stress distribution based on the limit equilibrium analysis (USCOE, 2008) that did not consider the existence of piles and sheet piles. Two results agree fairly well above the projected failure line. However, a substantial difference is observed below the projected failure line; the computed results in this study show that substantial normal stresses act even at deeper depths while limit equilibrium method does not show any stresses. Therefore it is inferred that the limit equilibrium approach may not provide accurate and pile analysis. Furthermore, it may results in a non-conservative computation.

To evaluate the factor of safety for bearing stress in front of the piles,  $P/P_u$  (where,  $P$ =lateral stress,  $P_u$ =ultimate lateral bearing capacity) is plotted in Fig. 11. It shows that the overall  $P/P_u$  is lower than 0.1 and the maximum  $P/P_u$  is lower than 0.3, indicating soils in front of the pile has factor of safety higher than 3.3 in terms of the bearing stress.

Fig. 12 shows the computed axial pile stress for piles in the front row and middle row. Axial pile stress is caused from both the axial forces and the bending moments. Large

compressive stress is generated in the middle row piles, and large tensile stress is generated in the front row piles. The result of back row piles is not shown but they showed smaller compressive and tensile stresses compared to previous two cases. The yield stress of the standard H-pile is  $345 \text{ MN/m}^2$  (A572 Grade 50). The maximum stress of piles obtained from FLAC<sup>3D</sup> is  $53.0 \text{ MN/m}^2$ , which is much lower than the yield stress of H-piles. Therefore, it shows that the H-piles are in safe condition.

Fig. 13 shows the variation of the lateral displacement with depth. The lateral displacement obtained from this study is significantly larger than the lateral displacements obtained from USCOE (2008). Particularly, the lateral displacement at deeper depth is higher than the one from USCOE (2008). This is because USCOE (2008) implicitly assumed zero lateral stress acting on the pile below the failure line while this study included it in the computation as addressed in Fig. 10. The lateral displacement at the pile tip is about 1.5 cm, however, it is noted that the soil deformation around the pile tip is 1.2 cm to 1.4 cm range. Therefore, the substantial portion of this much lateral deformation is due to the overall soil deformation, not the relative displacement between the pile and soils. The relative lateral displacement of piles must be the magnitude in Fig. 13 minus 1.2 to 1.4 cm. The shape of the lateral deformation at shallower depths is also different from that of USCOE (2008), because this study considers realistic pile/cap connections and rotational soil deformations at shallow layers as shown in Fig. 9.

*Stability of T-wall and pile stress for weaker soil conditions*

In simulating T-wall systems so far, representative soil properties were used. However, it is possible to encounter weaker soil conditions in the field, and the stability of the T-wall may not be guaranteed. Therefore, additional numerical simulations are performed for the same mesh but with reduced soil strengths and moduli up to one half the initial values. This much reduction is possible considering the scatter of field strength data shown in IPET (2007). Fig. 14 shows the comparison of peak axial pile stress normalized with the allowable stress of the H-pile for various soil strength conditions. It shows the stress level in the H-pile is increased when shear strength of soils is reduced, but still lower than the allowable stress. The lateral displacement is increased when shear strengths of soils are reduced. But the increased displacement did not indicate the instability of piles. Therefore, it seemed that H-piles perform reasonably well even when the strength of soils is reduced up to 50%.

#### *Stability of two row piled T-wall system*

A number of T-walls in New Orleans have two-row piles, so the safety of a T-wall having two-row piles is studied. An analysis is conducted on two row piled T-wall with the soil and other conditions the same as the three-row piled T-wall. The lateral displacement of the two-row piled T-wall is higher by 38.2 % than that of the three-row piled one. However, the maximum pile stress is increased only by 6.5 %, indicating the pile stress is still lower than one half the allowable pile strength.

#### *Flow through effect*

Flow of soils between piles may occur when the shear strength of soils is low and the stress level is high enough to cause the overall yield for soils. For the case of the T-wall section used in this study, the possibility of “flow through” is evaluated by checking the yielded element underneath the T-wall.

Fig. 15(a) shows that there are no yielded elements for a T-wall with soil data shown in Table 1 and when the water table is at EL. 3.0m. Fig. 15(b) shows the yielded elements when shear strength of the soils was reduced to one half their actual strengths; it shows that there are some sporadically distributed yielded elements, not showing the sign of overall failure.

Fig. 16(a) shows the yielded elements when there are no sheet piles or batter piles. For this case, soils underneath the T-wall failed along the curved failure line even at the water level EL. 1.8 m. When the water table is at EL. 1.8 m, the continuous deformation is observed in “zone of high shear strain rate” in Fig. 16(a). When sheet piles are added, the massive yielded elements and “zone of high shear strain rate” are observed in Fig. 16(b) at the water level EL. 2.4 m., showing the massive flow behavior.

Contrary to the results of limit equilibrium analysis (FS=1.02 based on USCOE, 2008), results in Figs. 16 show that the T-wall without the batter piles fails at the lower water level. It is noted that the limit equilibrium analysis assumed that the water pressure acting on the T-wall (concrete structure) is carried solely by the batter piles and water pressure acting on the soil is carried solely by the soils; no interaction between soils and piles are considered. They are, however, considered in this study.

From Figs. 15 and 16, it is shown that soils underneath the T-wall are weak enough to develop the “flow-through” effect; however the sheet piles and batter piles are holding soils so that it does not “flow through.”

### *Stresses in concrete walls*

The stresses in the concrete wall and base showed maximum compressive stress 2.16 MPa and maximum tensile stress 2.42 MPa as shown in Fig. 16. These numbers are lower than the estimated compressive strength (28.3 MPa, IPET 2007) and tensile strength (3.4 MPa, IPET 2007) of the concrete. It is noted that the numerical simulation was performed using homogenized reinforced concrete (Modulus of the wall material was computed based on the weighted average of concrete and reinforcing bars), the actual concrete stress must be even lower than the numbers appeared in Fig. 16. Therefore, it is shown that the overall stress condition for the concrete wall is below the yield stress of the system.

### **Summary and Conclusion**

In this study the behavior of a T-wall system in New Orleans was investigated through the three dimensional numerical analysis using FLAC<sup>3D</sup> accounting for three dimensional soil structure interactions and explicit/implicit loading conditions. Many scientific findings are listed as follows,

- 1) The normal lateral spring constants for a pile element in a passive pile condition were estimated by comparing applied lateral displacements and induced lateral forces at each depth. The ultimate soil resistance of a passive pile turned out to be  $P_u \approx 9 s_u$  for a circular pile and  $P_u \approx 15 s_u$  for a rectangular pile, which showed good agreement with published results.
- 2) With the pile element, creating a 3D mesh was very convenient, and it took only about 1/5 the computation time required for full 3D solid element simulations. In addition, the results of the pile element analyses in a passive pile condition were almost identical to the 3D solid element analyses when appropriate soil spring constants are used.
- 3) The overall deformation shape resembled that of the slope instability type ground deformation. This rotational motion conceptually agreed well with critical failure surface predicted by the limit equilibrium, but not with the conventional design concepts (USCOE, 1967) which did not consider the slope stability problems.
- 4) The magnitude of lateral stresses acting above the projected slope failure line was about the same as the one predicted using the limit equilibrium based slope stability analysis; however, a substantial difference was observed below the projected failure line. The computed results in this study showed that substantial normal stresses act even at deeper depths while limit equilibrium method did not show any stresses. Therefore, the limit equilibrium based slope stability analysis resulted in non-conservative design for the T-wall system.
- 5) The factor of safety for lateral bearing failure in front of the pile was higher than 3.3.
- 6) The lateral displacement obtained from this study (Max.  $\approx 6.1$  cm) is significantly larger than the lateral displacement obtained from USCOE (2008) (Max.  $\approx 1.2$  cm). This was due

to the fact that USCOE (2008) implicitly assumed zero lateral stress acting on the pile below the failure line while this study included it in the computation.

- 7) Even when soil strengths and moduli were reduced up to one half the initial values, axial stresses in piles were still within the allowable stress limit. The lateral displacement was increased with reduced shear strengths. But the increased displacement did not indicate the instability of piles.
- 8) The lateral displacement of the two-row piles was higher by 38.2 % than that of the three-row piles. However, the maximum pile stress increased only by 6.5 %, indicating the pile stress was still lower than one half the allowable pile strength.
- 9) Soils underneath the T-wall were weak enough to develop the “flow-through” effect; however the sheet piles and batter piles were holding soil movements so that the soils do not “flow through.”
- 10) The stresses in concrete wall and base showed maximum compressive stress 2.16 MPa and maximum tensile stress 2.42 MPa, lower than both for the compression and tension yield strengths.

The above conclusions are derived only for T-walls with steel H-piles. Behavior of T-walls with concrete piles is under study and will follow this paper in the near future.

### **Acknowledgements**

This work was supported by the funding received under a subcontract from the Department of Homeland Security-sponsored Southeast Region Research Initiative (SERRI) at the Department of Energy’s Oak Ridge National Laboratory, USA.

## References

- Adhikari, S., Song, C. R., Cheng, A. H. D., and Al-Ostaz, A. (2009). "2-D numerical simulation of I-wall for retrofitting design of flood protection systems in New Orleans." The 3<sup>rd</sup> annual DHS University Network Summit, March, Washington DC.
- Brandon, T. L., Wright, S. G., and Duncan, J. M. (2008). "Analysis of the Stability of I-Walls with Gaps between the I-Wall and the Levee Fill." *J. Geotech. Geoenviron. Eng.*, 134(5), 692-700.
- Bransby, M. F. and Springman, S. (1999). "Selection of load-transfer functions for passive lateral loading of pile groups." *Comput. Geotech.*, 24(3), 155-184.
- Broms, B. B. (1964). "Lateral resistance of piles in cohesive soils," *J. Soil Mech. Found. Div. Am. Soc. Civ. Eng.*, 90(2), 27-63.
- Chen, C. Y. and Martin, G. R. (2002). "Soil-structure interaction for landslide stabilizing piles." *Comput. Geotech.*, 29(5), 363-386.
- Chen, L. F. (1994). "The effect of lateral soil movements on pile foundation." PhD thesis, Univ. of Sydney, Australia.
- Coyle, H. M. and Sulaiman, I. H. (1967). "Skin friction for steel piles in sand." *J. Soil Mech. Foun. Div.*, 92(SM2), 1-26.
- Duncan, J. M., Brandon, T. L., Wright, S. G., and Vroman, N. (2008). "Stability of I-Walls in New Orleans during Hurricane Katrina." *J. Geotech. Geoenviron. Eng.*, 134(5), 681-691.
- Geomatrix. Inc. (2007) "Soil-Structure Interaction and Load Transfer Mechanism of Pile-Supported T-Wall for New Orleans Levees."
- Hartman, J. P., Jaeger, J. J., Jobst, J. J., and Martin, D. K. (1989). "User's Guide: Pile Group Analysis (CPGA) Computer Program," Technical Report ITL-89-3, US Army Engineer Waterways Experiment Station, Vicksburg, MS.
- Hrennikoff, A. (1949). "Analysis of pile foundations with batter piles." *American Society of Civil Engineers*, Transactions, Paper No. 2401, 351-374.
- Hurricane Protection Office (2008). "The London avenue site specific load test -Appendix D. Analysis of the London avenue canal load test - Section 1Soil structure interaction analysis." *Final Rep. of the Hurricane Protection Office of the US Army Corps of Engineers and St. Louis District Corps of Engineers*. U.S. Army Corps of Engineer.
- Interagency Performance Evaluation Task Force (IPET). (2007). "Performance evaluation of the New Orleans and Southeast Louisiana Hurricane protection System." *Final Rep. of the Interagency Performance Evaluation Task Force*, U.S. Army Corps of Engineer.

Itasca. (2006). *FLAC<sup>3D</sup>. Fast Lagrangian analysis of continua, version 3.1*, Structural element manual. Itasca, Minnesota, 178-183.

Jaky, J. (1944). "The coefficient of earth pressure at rest," *Journal of Hungarian Architects and Engineers*, Budapest, Oct., 355-358.

Martin, G. R. and Chen, C. Y. (2005). "Response of piles due to lateral slope movement." *Computers and Structures*, 83, 588-598.

Matlock, H. (1970). "Correlations for design of laterally loaded piles in soft clay," *Paper No. OTC 1204. Proc., 2nd Annual Offshore Technology conf.*, Houston, 1, 577-594.

Meyerhof, G.G. (1976), "Bearing capacity and settlement of pile foundations," *J. of Geotech. Eng.*, ASCE, 102(GT3), 197-228.

Pan, J. L., Goh, A. T. C., Wong, K. S., and Teh, C. I. (2002). "Ultimate soil pressure for piles subjected to lateral soil movements." *J. Geotech. Geoenviron. Eng.*, ASCE, 128(6), 530-535.

Poulos, H. G. (1995). "Design of reinforcing piles to increase slope stability." *Can. Geotech. J.*, 32(5), 808-818.

Randolph, M. F., and Houlsby, G. T. (1984). "The limiting pressure on a circular pile loaded laterally in cohesive soil." *Geotechnique*, 34(4), 613-623.

Reese, L.C. and O'Neill, M.W. (1989), "New Design Method for Drilled Shafts from Common Soil and Rock Tests," *Proceedings, Foundation Engineering: Current Principles and Practices*, ASCE, 2, 1026-1039

Reese, L. C. and O'Neill, M. W. (1988). "Drilled shafts: Construction Procedures and Design " FHWA, Publication No. HI-88-042

Reese, L. C. and Wang S. T. (2007). "Group 7 for Windows, Analysis of a group of piles subjected to axial and lateral loading." Ensoft, Inc., Austin, TX.

Spencer, E. (1967). "A method of analysis of the stability of embankments assuming parallel inter-slice forces." *Geotechnique*, 17(1), 11-26.

US Army Corps of Engineer (2008). *Hurricane and Storm Damage Reduction System Design Guidelines (HSDRS DG)* - New Orleans District Engineering Division.

US Army Corps of Engineer (1991). *Design of Pile Foundations*. EM 1110-2-2906. Chap 4. 1-27.

US Army Corps of Engineer (1967). *Lake Pontchartrain, LA. And Vicinity Lake Pontchartrain Barrier Plan, Design Memorandum No.2, General Advance Supplement, Inner Harbor Navigation Canal West Levee, Florida Avenue to IHNC Lock*, March. 18-23.

Vetter, C. P. (1939). "Design of pile foundations." *American Society of Civil Engineers, Papers*, 311-331.

Viggiani, C. (1981). "Ultimate lateral load on piles used to stabilize landslides." *Proc., 10th Int. Conf. on Soil Mechanics and Foundation Engineering*, Stockholm, A.A. Balkema, Orterdam, The Netherlands, 3, 555-560.

Table 1. Soil Properties

Layer	Top elev. (m)	Soil type	$s_u$ (kN/m <sup>2</sup> )	$s_u/z$ (kN/m <sup>2</sup> /m)	$\phi$ (degree)	$\gamma$ (kN/m <sup>3</sup> )	$G/s_u$	G (kN/m <sup>2</sup> )	K (kN/m <sup>2</sup> )
Levee fill	0.3		23.9			17.3	150	3585.0	8.86e4
Peat	-0.6	CH	5.7			12.6	100	574.6	1.42e4
Clay 1	-4.3	CH	7.2			15.7	130	933.7	2.30e4
Clay 2	-7.0	ML	9.6		15	18.4	130	1244.9	3.07e4
Clay 3	-7.9	CH	9.6			15.7	130	1244.9	3.07e4
Clay 4	-9.4	CH	9.9	1.27		15.7	130	1350.2	3.33e4
Clay 5	-11.9	CH	17.9	1.30		15.7	160	2863.2	7.09e4
Clay 6	-21.3	CH	37.8			15.7	160	6032.9	1.49e5
Sand	-26.2	SP	N.A.		30	18.1	N.A.	7804.4	1.69e4
Clay	-33.8	CH	46.9	1.30		18.1	160	7517.2	1.85e5

$s_u$  = undrained shear strength,  $s_u/z$  = increment of undrained shear strength with depth,  $\phi$  = friction angle,  $\gamma$  = unit weight,  $G/s_u$  = modulus to strength ratio, G = shear modulus, and K = bulk modulus.

Table 2. Strength parameters of normal coupling springs

Layer	Elev. (m)		$c_n$ (kN/m)	$\phi_n$ (degree)	$k_n$ (MN/m/m)
	Top	Bottom			
Peat	-1.5	-4.3	24.6	11.8	2.0
Clay 1	-4.3	-7.0	16.8	21.8	2.6
Clay 2	-7.0	-7.9	170.6	0.0	3.0
Clay 3	-7.9	-9.4	3.4	33.7	4.9
Clay 4	-9.4	-11.9	3.4	33.7	4.9
Clay 5	-11.9	-21.3	0.0	45.0	12.3
Clay 6	-21.3	-26.2	0.7	40.8	37.2
Sand	-26.2	-27.7	465.3	33.1	54.5

Table 3. Properties of structures

Structures	Element	Structural properties			Interface properties						
Sheet pile	Embedded liner	E	200	GN/m <sup>2</sup>	k <sub>n</sub>	Varies with depth (Eq. 4)					
		v	0.3								
		Thickness	1.21*	m	k <sub>s</sub>						
		Density	3.5								
Concrete T-wall	Brick element	G	9.6	GN/m <sup>2</sup>	k <sub>n</sub>	2.12	GN/m <sup>2</sup> /m				
		K	27.6	GN/m <sup>2</sup>	k <sub>s</sub>	2.12	GN/m <sup>2</sup> /m				
		Density	4.32		c <sub>i</sub>	3.82	kN/m <sup>2</sup>				
					φ <sub>i</sub>	0	Degree				
H-piles	Pile element	E	200	GN/m <sup>2</sup>	c <sub>n</sub>	Varies with depth (Table 2, Eq. 2)					
		v	0.3		φ <sub>n</sub>						
		Area	0.0138	m <sup>2</sup>	k <sub>n</sub>						
		I <sub>y</sub>	3.03e-4	m <sup>4</sup>	c <sub>s</sub>						
		I <sub>x</sub>	1.09e-4	m <sup>4</sup>	φ <sub>s</sub>						
		I <sub>j</sub>	4.12e-4	m <sup>4</sup>	k <sub>s</sub>						
		Perimeter	1.43	m	Tip		Area	0.127	m <sup>2</sup>		
							Q**	535.0	kN		
							K**	48.0	MN/m		
							Head		Area	0.127	m <sup>2</sup>
									Q**	4.2	MN
					K**	4.4	GN/m				

\* Thickness of a sheet pile represents equivalent thickness which provides the same flexibility (EI).

\*\* Q = ultimate capacity of endbearing spring; K = stiffness of endbearing spring.

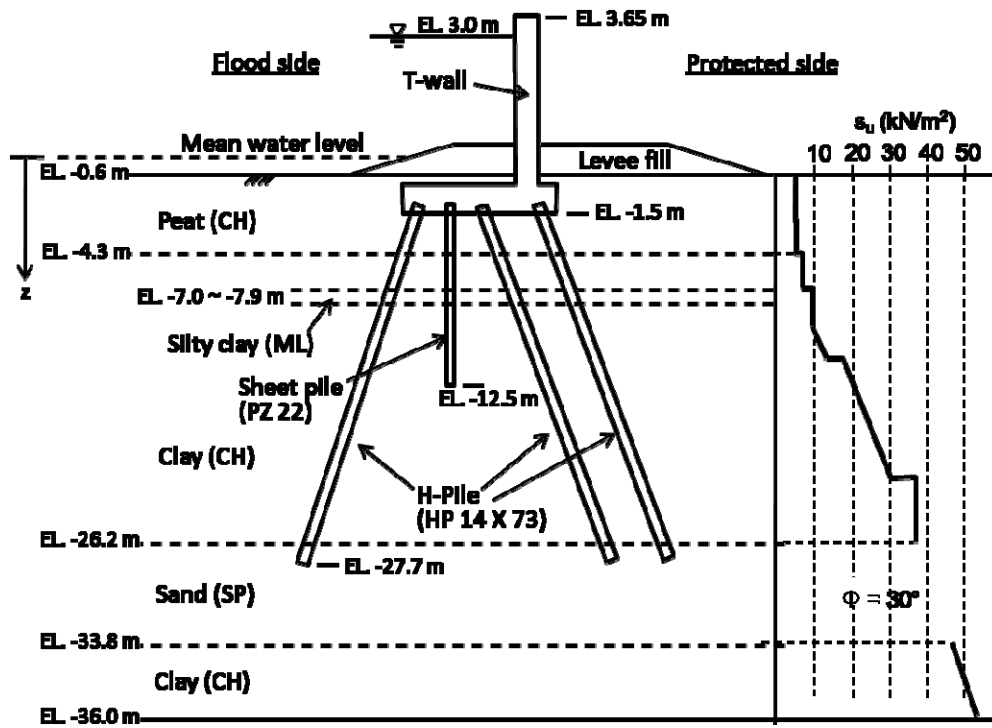


Fig 1. T-wall and soil profile in New Orleans' IHNC (USCOE, 2008)

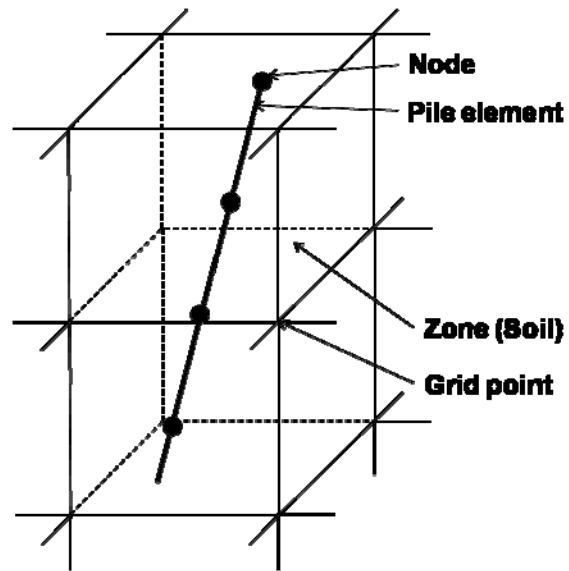


Fig 2. Pile element in FLAC<sup>3D</sup>

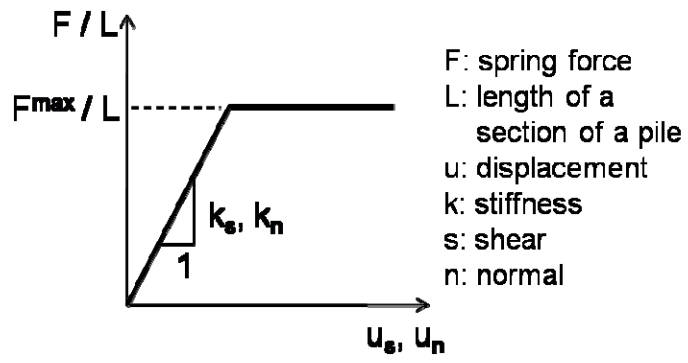


Fig 3. Bi-linear coupling spring models in a pile element

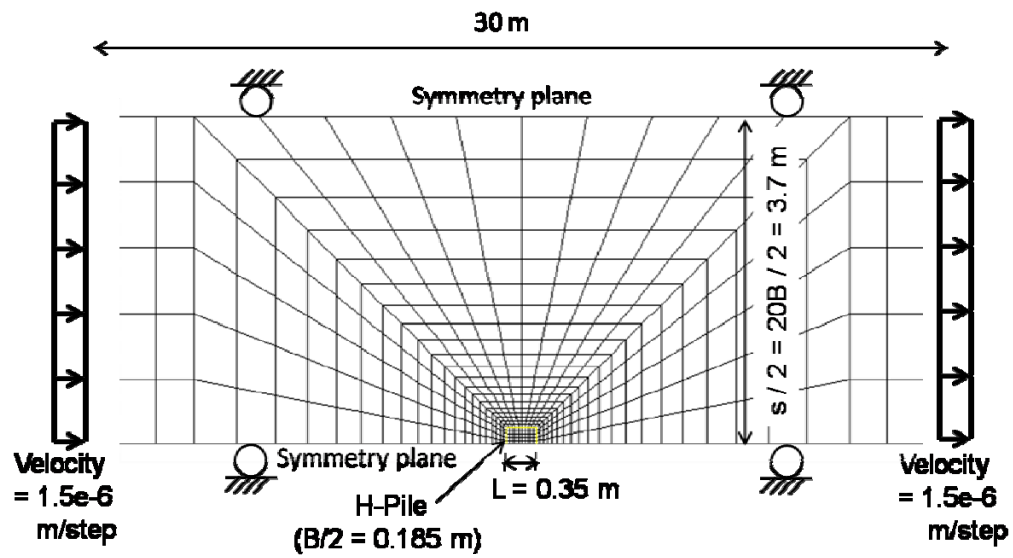


Fig 4. Mesh of plane strain analysis for estimating normal coupling spring properties at a certain depth

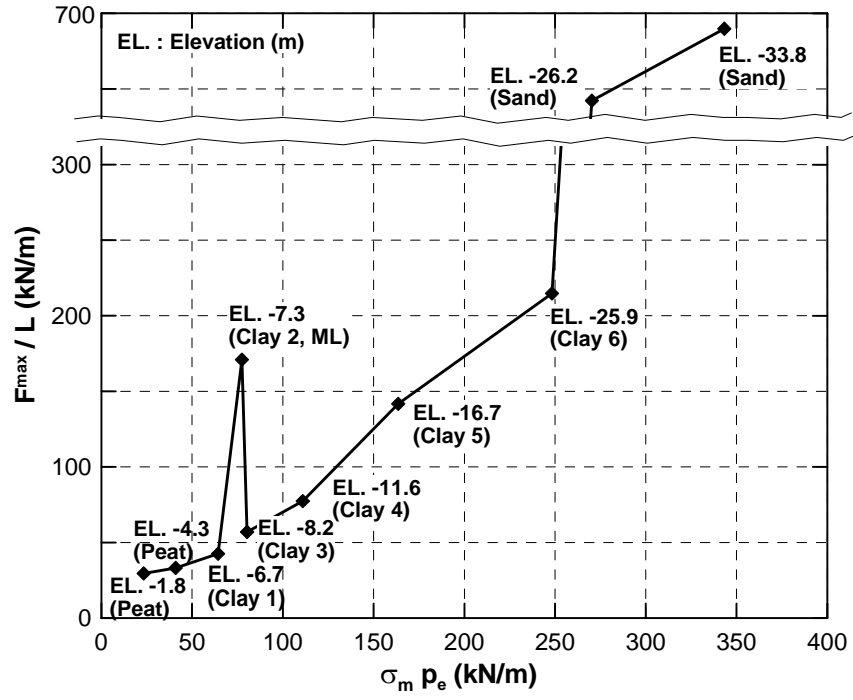
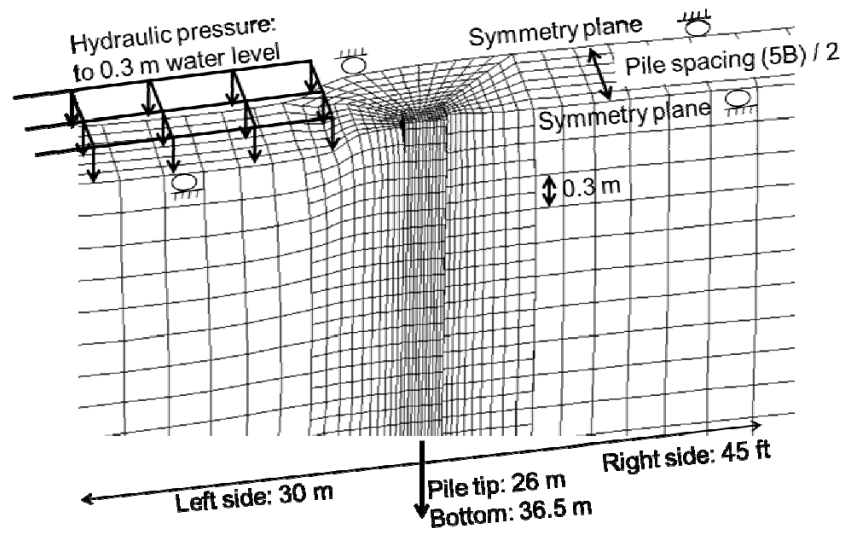
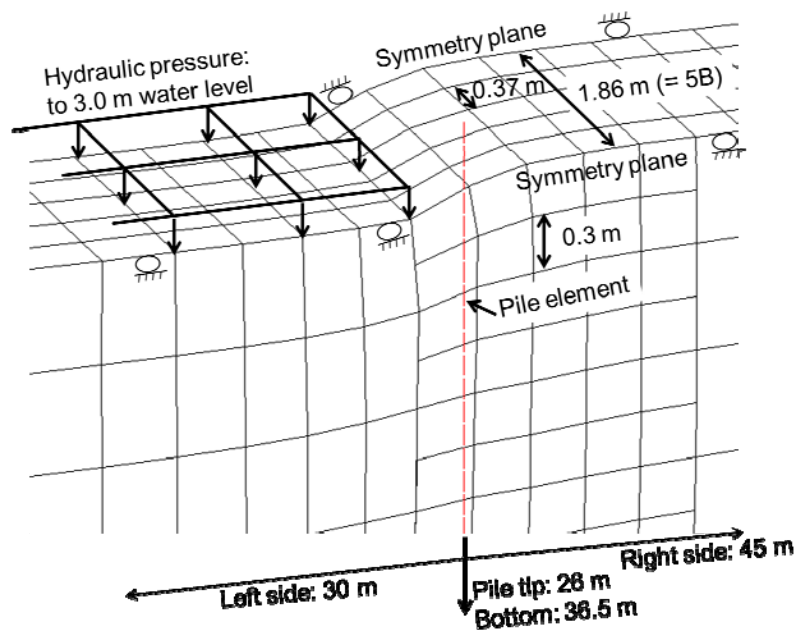


Fig 5. Normal coupling spring constants



(a) Mesh with 3D solid element



(b) Mesh with pile element

Fig 6. Two deformed meshes of H-pile in passive case ( $s / B = 5$ , Deformation exaggerated 3 times)

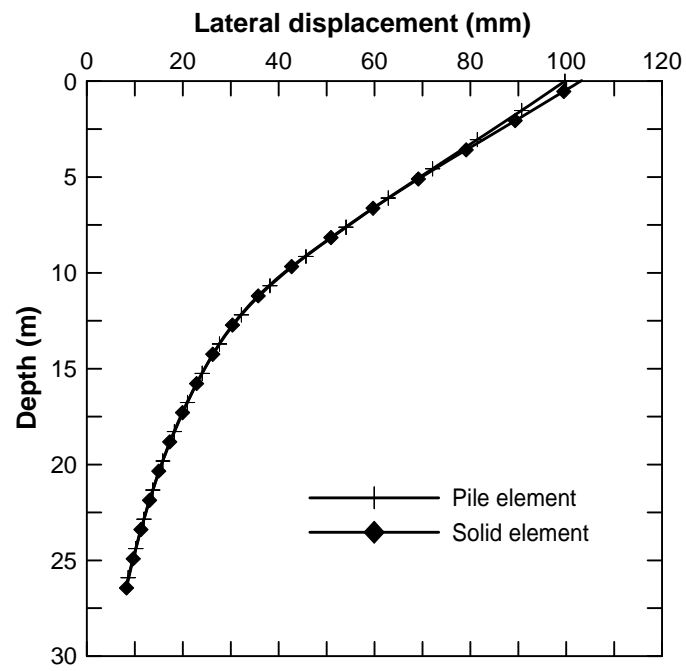
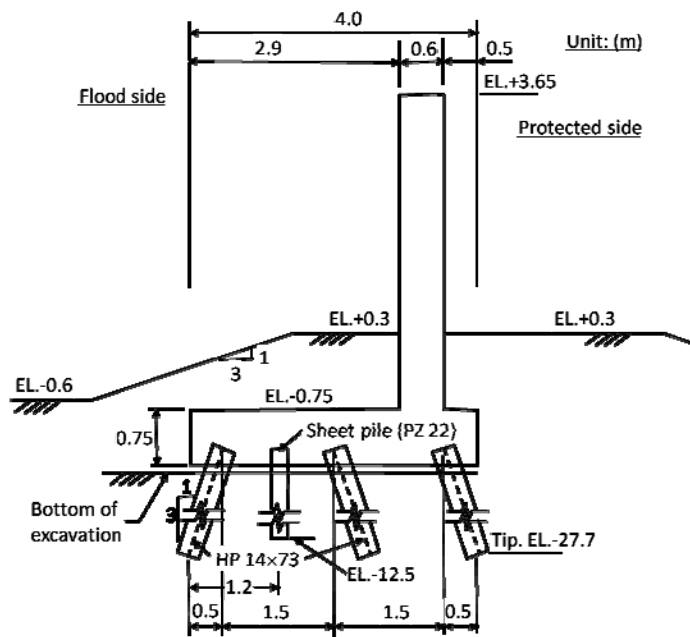
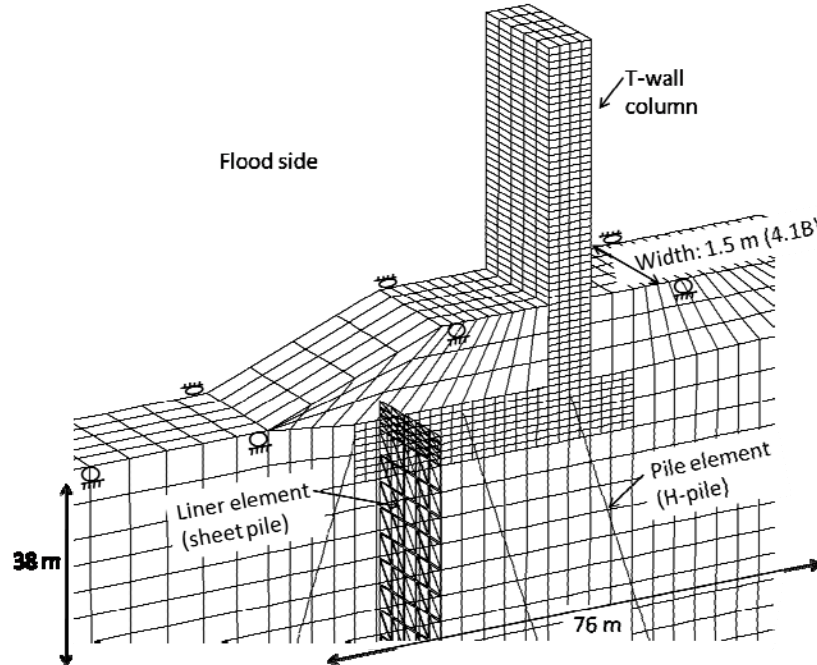


Fig 7. Comparison of lateral displacement with depth for pile element and 3D solid element



(a) Details of T-wall structure



(b) 3D mesh of T-wall system

Fig 8. Modeling of T-wall

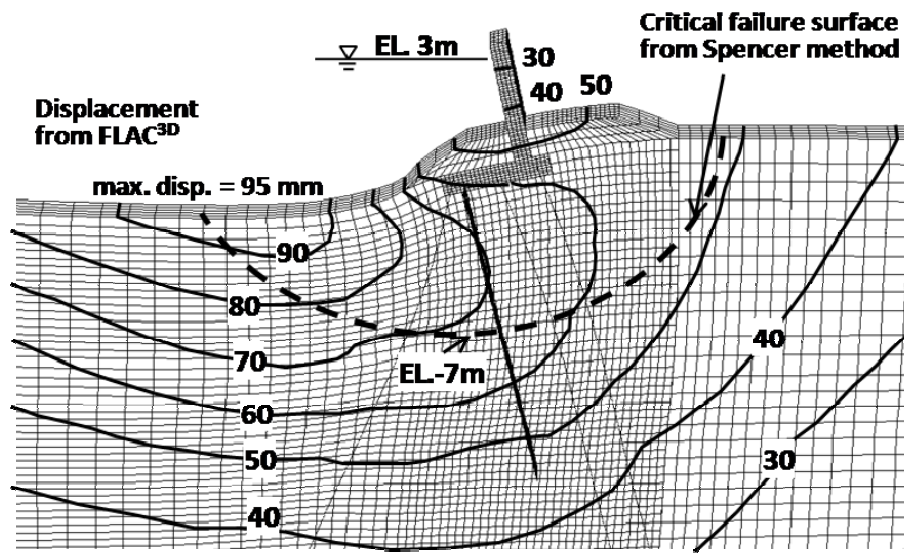


Fig 9. Displacement contour from FLAC and critical surface from Spencer's method with 3 m water level (Deformation exaggerated 30 times)

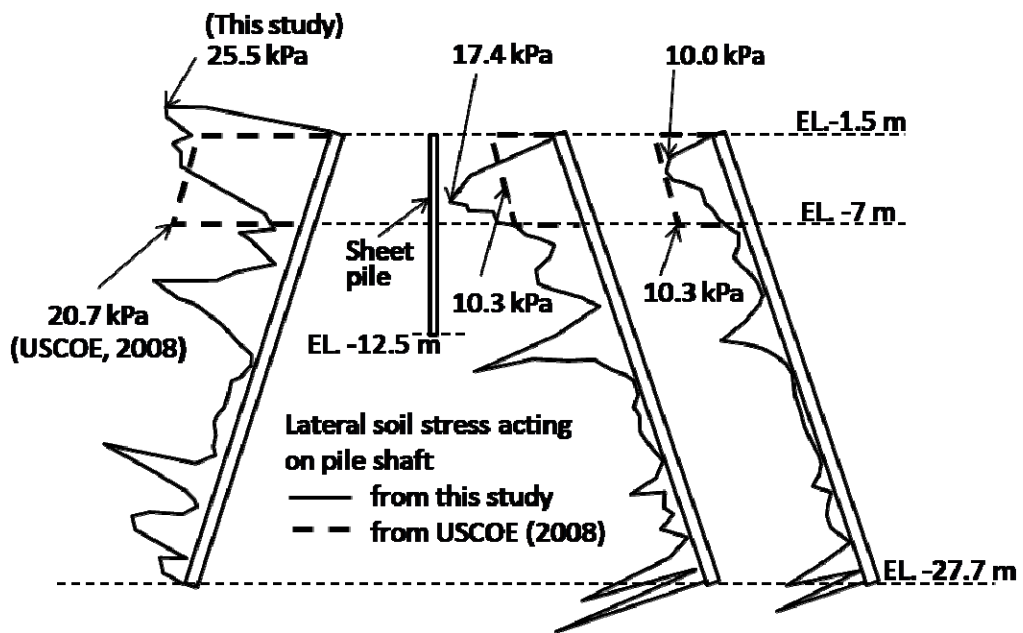


Fig 10. Lateral soil stress acting on pile shafts

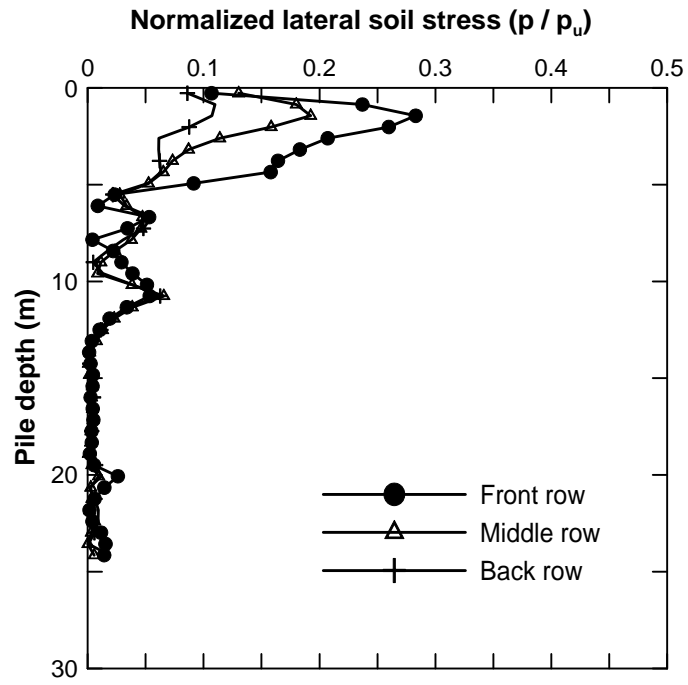
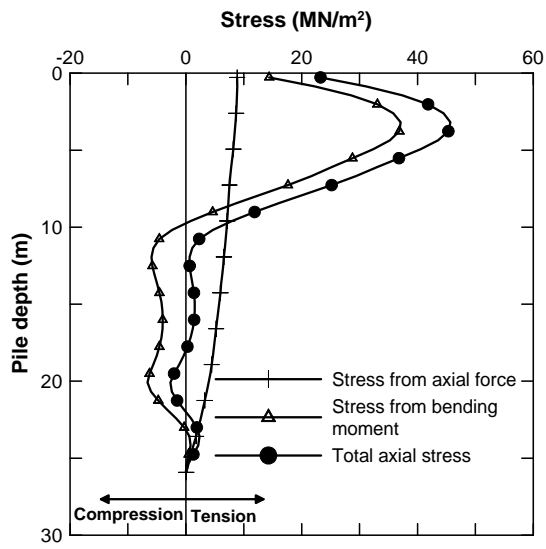
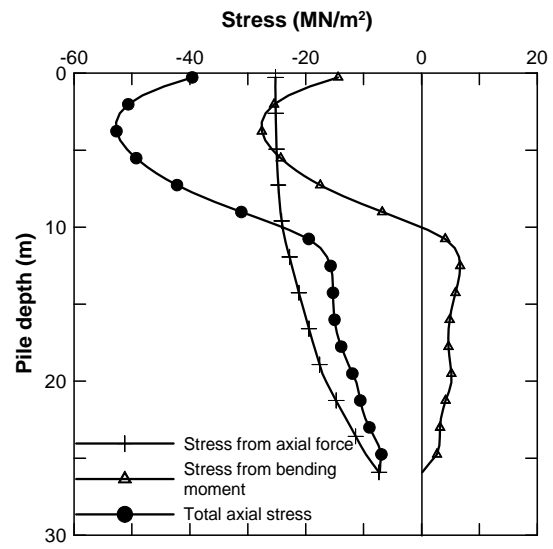


Fig 11. Normalized normal stress acting on pile shaft



(a) Front row



(b) Middle row

Fig 12. Axial pile stresses

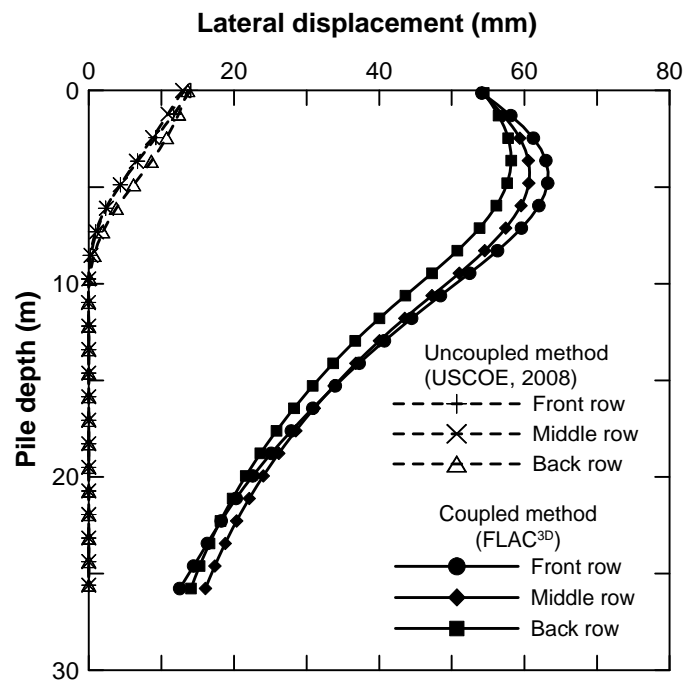


Fig 13. Comparison of displacement with the results of design guideline

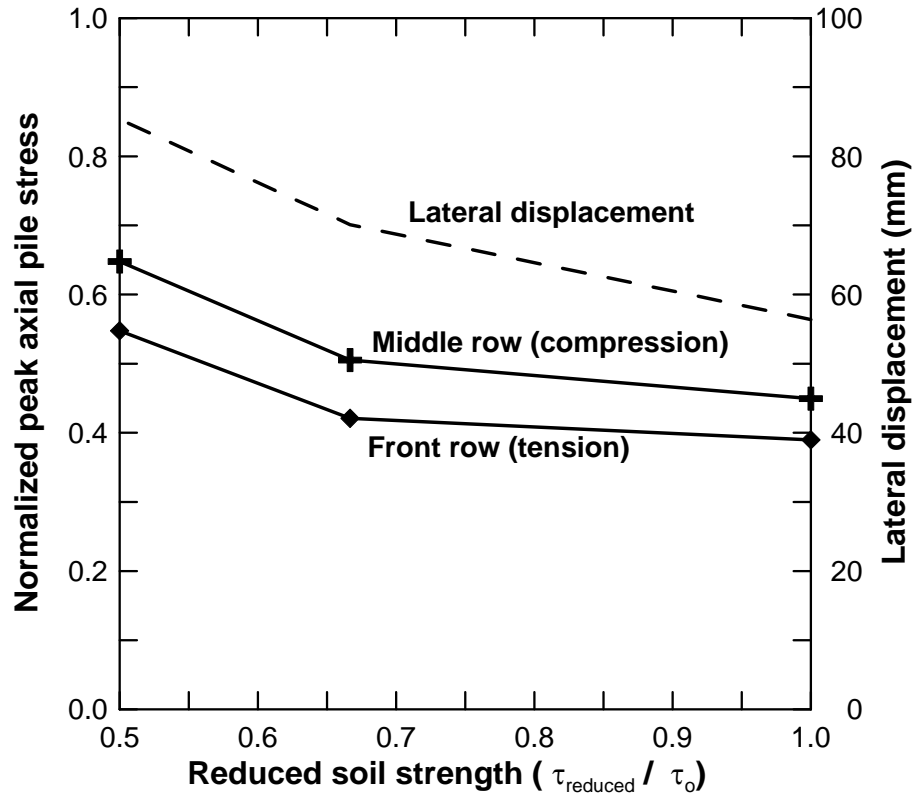
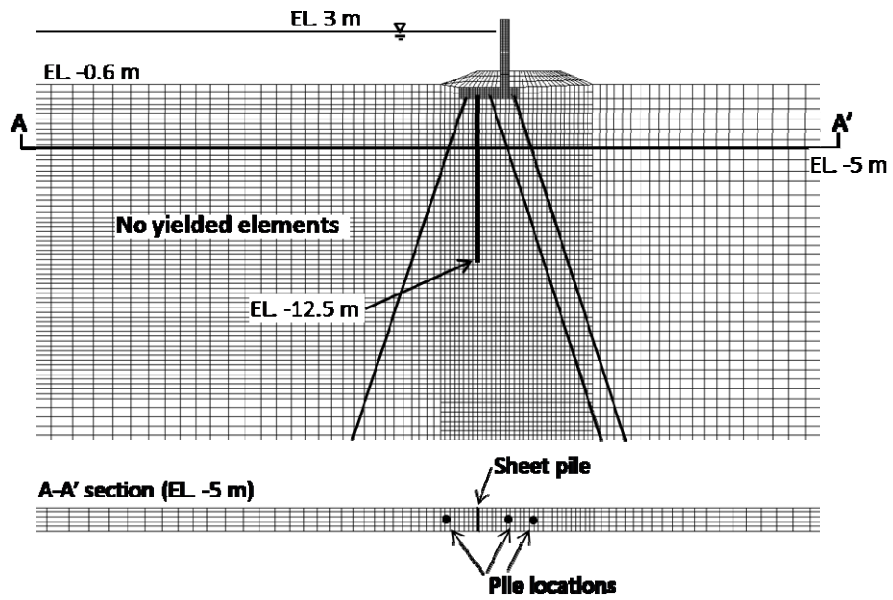
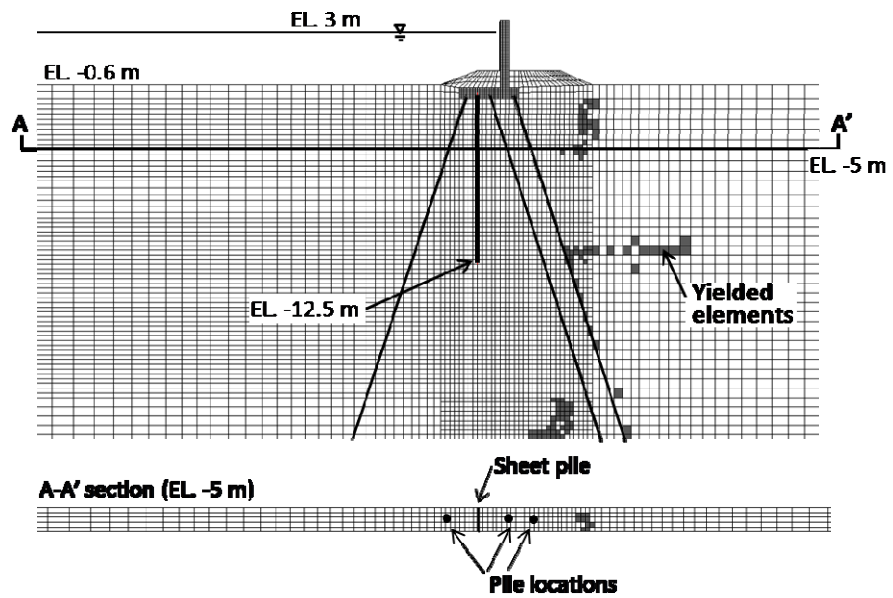


Fig 14. Normalized peak axial pile stress and lateral displacement with reduced soil properties

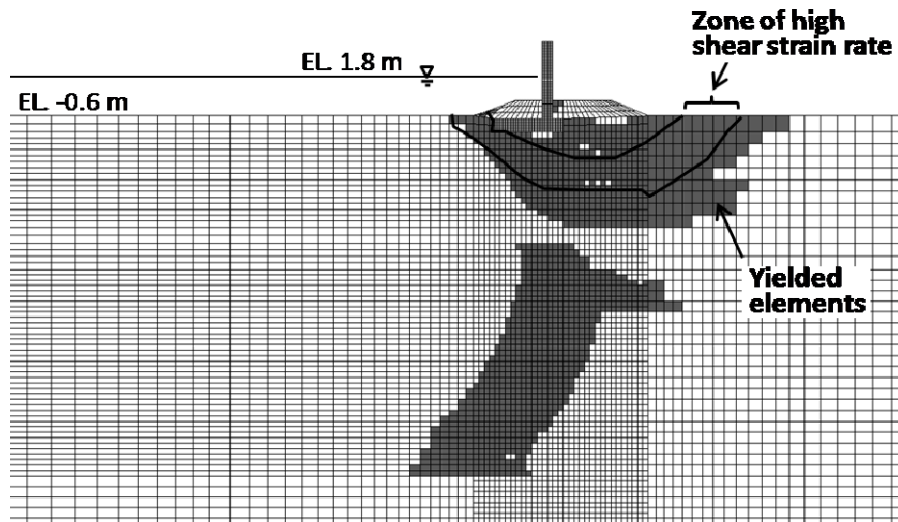


(a) Yielded soil elements with unfactored soil data

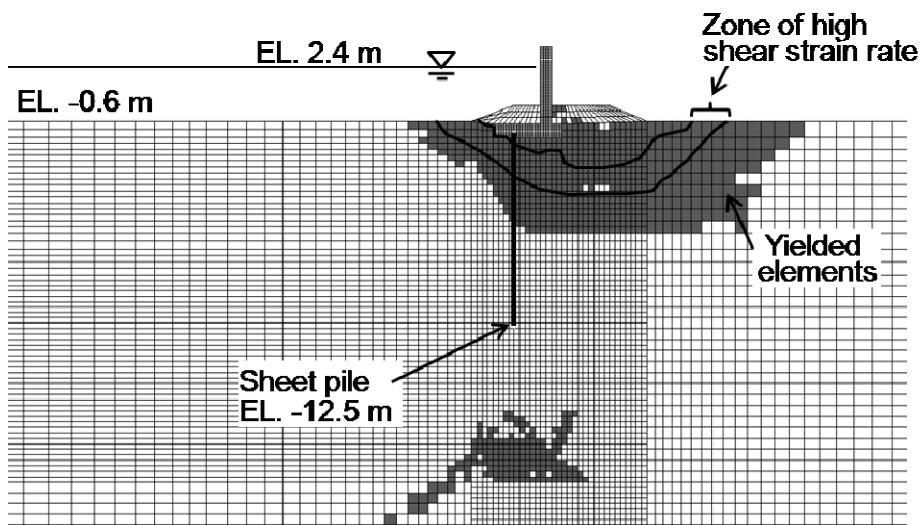


(b) Yielded soil elements with one-half shear strength

Fig 15. Yield zone of soil at 3 m water level



(a) T-wall with no piles and no sheet piles



(b) T-wall with sheet piles

Fig 16. Yielded zone of soils for a T-wall section

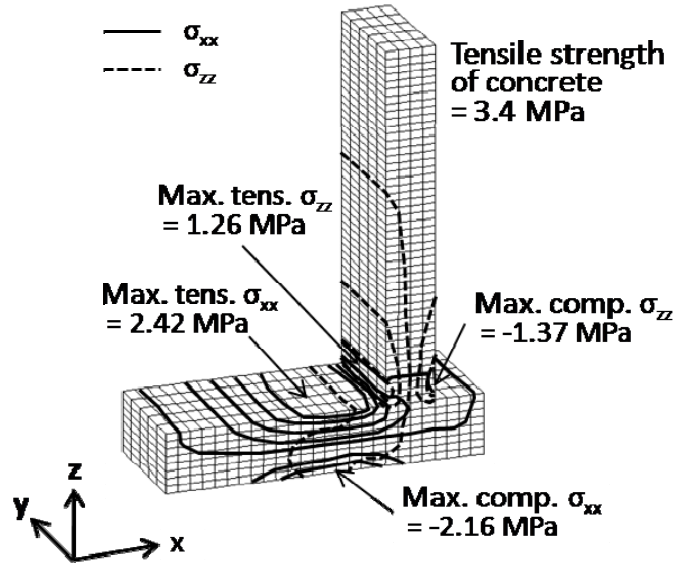


Fig 17. Stress levels in the concrete wall (Simulation conducted for mesh appeared in Fig. 8(b) but results appeared only for the concrete wall)